

Carbon Fibers Enhance the Propagation of High Loading Nanothermites: In Situ Observation of Microscopic Combustion

Haiyang Wang, Dylan J. Kline, Miles C. Rehwoldt, and Michael R. Zachariah*

Cite This: *ACS Appl. Mater. Interfaces* 2021, 13, 30504–30511

Read Online

ACCESS |



Metrics & More



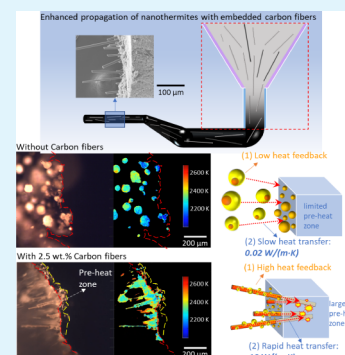
Article Recommendations



Supporting Information

ABSTRACT: A major challenge in formulating and manufacturing energetic materials lies in the balance between total energy density, energy release rate, and mechanical integrity. In this work, carbon fibers are embedded into ~90 wt % loading Al/CuO nanothermite sticks through a simple extrusion direct writing technique. With only ~2.5 wt % carbon fiber addition, the burn rate and heat flux were promoted >2×. In situ microscopic observation of combustion shows that the carbon fiber intercept ejected hot agglomerates near the burning surface and enhanced heat feedback to the unreacted material. This study outlines how these approaches may enhance the propagation and reduce the two-phase flow losses.

KEYWORDS: carbon fibers, Al/CuO, nanothermites, 3D printing, direct writing



1. INTRODUCTION

A major challenge in energetic materials (propellants, explosives, and pyrotechnics) lies in the fine balance among mechanical integrity, energy density, and energy release rate.^{1–4} Although some energetic materials, such as monomolecular explosives, can release their energy on very small timescales, these reactions are intrinsically limited in energy output based on their fixed stoichiometry and final products.^{1–4} Other materials, such as metastable intermolecular composites (MICs) or nanothermites, have a potentially higher energy output but react on a much longer timescale.^{1–13} Interestingly, when mixing the nanothermite with high explosives, the combustion of the nanothermite could induce the transition from deflagration to detonation of a submicron high explosive powder.^{14–16} The time over which the energy is released is critical to their effective use as a propellant or other niche application of energetic materials.

Loosely packed energetic powders can propagate from ~m/s to ~km/s with propagation velocities closely correlated with the packing density,^{5–7} but they lack the mechanical integrity necessary for many practical applications. Recent studies on MICs have shown that reducing component size,^{8,9} enhancing the contact between fuels and oxidizers,^{10–13} and/or increasing the ignitability of the fuels^{17–19} enhance their reactivity. Loose powders must ultimately be manufactured into free-standing architectures by incorporating different types of binders or architectures for any realistic application.^{20–23} Unfortunately, the incorporation of these energetic materials into dense structures can also inhibit their performance since their combustion becomes limited by binder decomposition and

phase transitions,^{24–26} ultimately leading to order-of-magnitude changes in the burn rate.^{27,28} This leads to even more parameters to balance—binder materials must be employed to make the materials safe and avoid accidents but must be used in as little quantity as possible to retain their potential energy release.^{20,29–31}

One approach for balancing the mechanical integrity, potential energy density, and energy release rate could be to incorporate additives. For example, replacing conventional binders with energetic ones^{22,32–37} or applying the catalyst embedded with ammonium perchlorate.^{38,39} Embedding reactive or metal wires is known to promote combustion.^{40–42} New techniques and formulations have been introduced to increase the energetic material content^{29,43} and control combustion behavior via alterations to the chemical content.^{44,45} However, since these materials largely rely on nanothermites as their primary energetic component to maximize energy release, it is possible that energy is being inefficiently coupled back into the system to promote propagation, given their longer reaction time.⁴⁶ Considering that energy release rates in propellants are determined by how fast reactions occur and how fast energy can be transferred to unreacted material, one could feasibly use thermally con-

Received: February 16, 2021

Accepted: June 13, 2021

Published: June 25, 2021



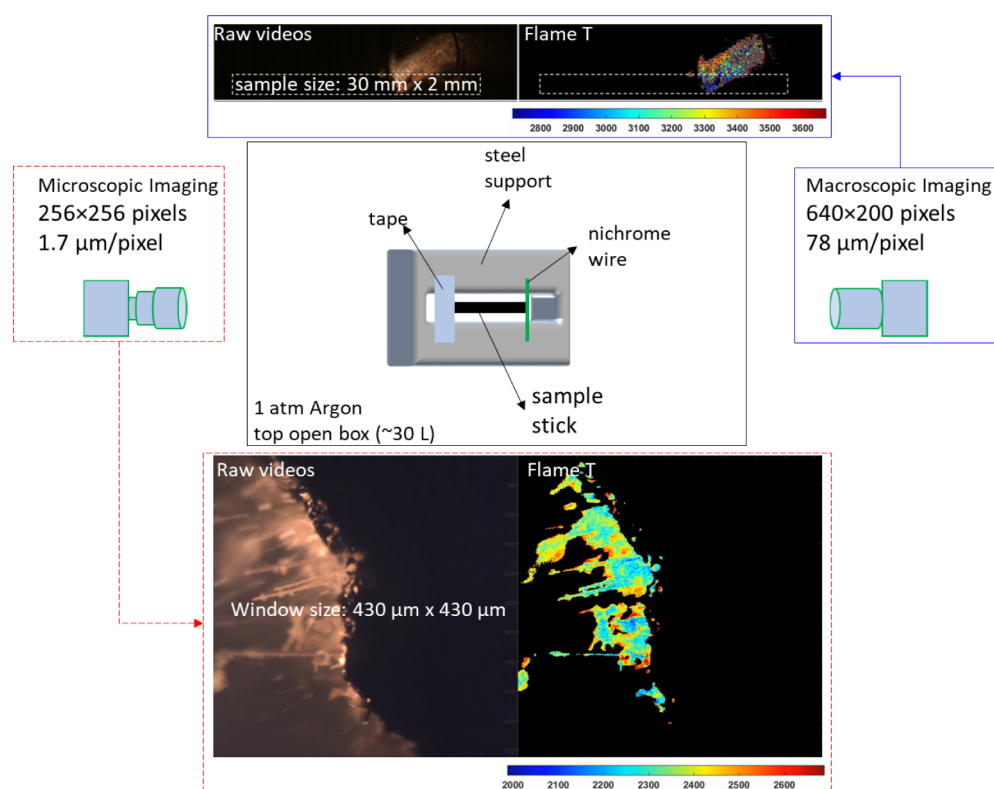


Figure 1. Schematic showing the setup and microscopic and macroscopic imaging of free-standing Al/CuO composite burning.

ductive materials as a method to improve the heat transfer and energy release rate.⁴⁷ Additionally, mechanical integrity may be bolstered by incorporating fibers that have been widely employed to reinforce polymer-based 3D structures.^{48–51} Should the thermally conductive additives be fibrous, they could serve the dual purpose of increasing both the mechanical integrity and the energy release rate.^{52–54} In this study, we choose carbon fibers as the additives as their high melting point (~ 3700 °C) should maintain their shape during the combustion and should have no catalytic effects (e.g., polymer decomposition or Al/CuO reaction).

In this work, carbon fibers were embedded into ~ 90 wt % loading Al/CuO nanothermite sticks through a simple direct writing approach. With the addition of only ~ 2.5 wt % carbon fibers, the propagation rate (burn rate) and heat flux of the sticks were promoted by $>2\times$. From in operando microscopic observations, the carbon fibers on the burning surface intercept ejected hot agglomerations, which can provide enhanced heat feedback to the unburnt materials on the flame front. This study provides insight into a new method to potentially accelerate the propagation of 3D-printed energetic composites.

2. EXPERIMENTAL SECTION

2.1. Materials. Aluminum nanoparticles (Al NPs, 67 wt % active, 81 nm) and CuO NPs (~ 40 nm) were purchased from Novacentrix Inc. and U.S. Research Nanomaterials, respectively. The active content of aluminum was measured by thermogravimetric analysis (TGA). METHOCEL F4M hydroxypropyl methylcellulose (HPMC) and polyvinylidene fluoride (PVDF) (average molecular weight: $\sim 534\,000$) were obtained from Dow Chemical Co. and Sigma-Aldrich, respectively. *N,N*-Dimethylformamide (DMF, 99.8%) was purchased from Sigma-Aldrich and used as a solvent to dissolve the above polymers. Carbon fibers were purchased from Composite Envisions. The physical properties of the carbon fibers are summarized in Table S1. SEM images and length distributions are

shown in Figure S1. In short, the diameter of the carbon fibers is ~ 7 μm , and they are chopped in a length of ~ 3 mm (labeled).

2.2. Ink Preparation. A detailed ink formulation with mass fractions of each composition is found in Tables S2 and S6. Table S2 provides the detailed mass fractions of each component with various carbon fiber additions (fixed equivalence ratio). Table S6 shows the formulations with different equivalence ratios (fixed carbon fiber addition). The ink formulating process is the same for the above two series of inks (Tables S2 and S6). Typically, 900 mg of Al and CuO, 50 mg of HPMC, 50 mg of PVDF, and 3.2 mL of DMF were used for each ink formulation. When preparing the inks, HPMC and PVDF were first added and dissolved in DMF in a mass ratio of 1:1 to form a clear viscous solution by magnetically stirring the mixture overnight (300 rpm). The carbon fibers were then added into the above solution (except for no carbon fiber cases) while being magnetically stirred to disperse the fibers. Then, certain amounts of CuO NPs and Al NPs were added into the above to form a slurry. A 30 min ultrasonication step was implemented after each addition of the CuO and Al NPs to break up aggregates. The slurries were magnetically stirred (300 rpm) for 24 h to achieve homogenization. After the last stirring step, the samples were ready to print.

2.3. Direct Writing Process. In the printing process, the obtained inks were extruded through a 16-gauge needle (purchased from McMaster-Carr, inner diameter: 0.053 in. (~ 1.35 mm)) at a feed rate of ~ 12 mL/h and printed into prepatterned (8 cm \times 8 cm square) lines on a preheated substrate kept at ~ 75 °C. The printing speed (moving speed of the nozzle) was 22 cm/min. The printed lines are ensured to be completely dry before depositing another layer, and the resulting lines (15 layers) formed a square 8 cm \times 8 cm frame with a thickness of ~ 1 mm and a width of ~ 1 mm (Figure S2). After printing, the samples were left on the heated substrate (kept at ~ 75 °C) for 30 min to further evaporate any remaining solvent. Finally, the frame was cut into 3 cm long sticks for combustion characterization (Figure 1). The density (mass/volume) is determined from the mass divided by the volume (cross-sectional area \times length) of each stick. The porosity of the samples was estimated by $(1 - (\text{actual density}/\text{theoretical density}))$. The

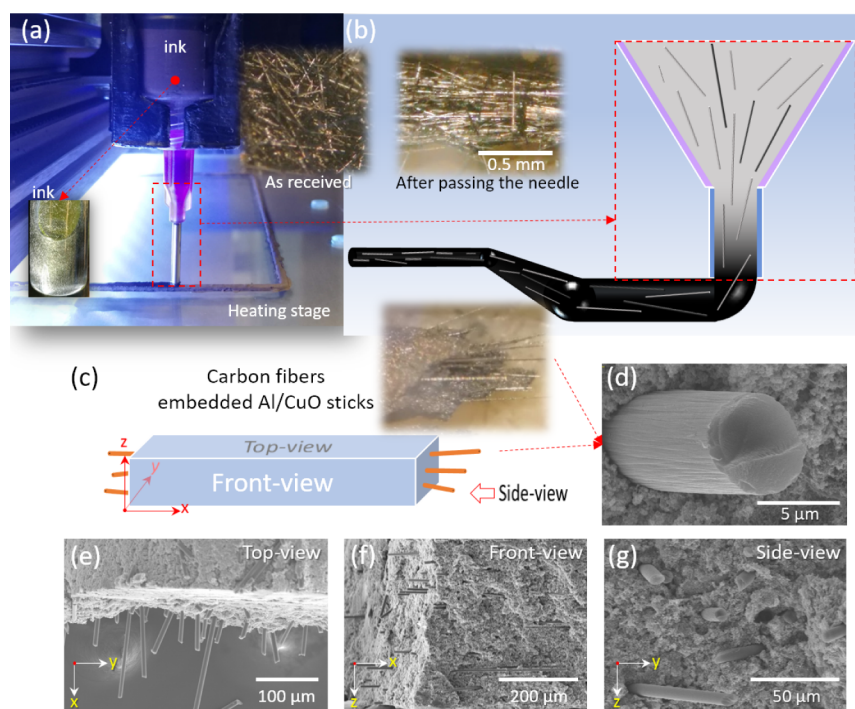


Figure 2. Optical image (a) and schematic showing (b) the direct writing process of Al/CuO composite sticks containing carbon fibers. Optical images of randomly dispersed (right inset in (a)) and aligned carbon fibers (inset in (b)). Prepared ink for direct writing with carbon fiber (left inset in (a)). Schematic (c) and optical image (inset in (c)) of Al/CuO (90 wt %) composite sticks with aligned carbon fibers. SEM images of Al/CuO composite with carbon fibers on side view (d,g), top view (e), and front view (f). Note: The amount of carbon fibers in the sticks shown in this figure is 2.5 wt %. The SEM images of other sticks (with different amounts of carbon fibers) are shown in Figure S2.

measured and theoretical densities/porosities of the sticks are summarized in Table S3, S7, and S8. The optical photos and cross-sectional SEM images of the sticks are shown in Figure S2.

2.4. Scanning Electron Microscopy/Energy-Dispersive X-ray Spectroscopy and Thermogravimetric/Differential Thermal Analysis. The morphologies and compositions of the carbon fibers and the 3D-printed composite sticks were characterized by scanning electron microscopy (SEM, Thermo-Fisher Scientific NNS450) coupled with energy-dispersive X-ray spectroscopy. TGA/differential thermal analysis (TGA/DSC, Proteus80 from NETZSCH) in this study was conducted in an argon flow (50 mL/min) at a heating rate of 10 °C/min from room temperature to 1000 °C.

2.5. Macroscopic and Microscopic Imaging. The experimental setup used in this study is shown in Figure 1. The samples are free-standing burn sticks (3 cm long, ~2 mm wide, and ~1 mm thick). The sample sticks were attached on a steel support that is mounted to a 3D translational stage (Newport). The whole stage was placed in a box (top open, volume: ~30 L), which would be filled with argon (1 atm) from the bottom before performing the burn test. The sample sticks were ignited by nichrome wire, as shown in Figure 1. Aside the argon box, there are two camera systems with different magnifications, which can be triggered simultaneously to get two videos for a single event at both macroscopic and microscopic views. The macroscopic imaging high-speed camera (78 $\mu\text{m}/\text{pixel}$, Vision Research Phantom Miro M110) captures the back view at a sample rate of 13 000 frames/s (640 \times 200 pixels), while a microscopic imaging system (~1.7 $\mu\text{m}/\text{pixel}$, Vision Research Phantom VEO710L coupled to Infinity Photo-Optical Model K2 DistaMax) captures the front view at a sample rate of 24 000 frames/s (512 \times 512 pixels).

2.6. Burn Rate and Flame Temperatures. The linear burn rate (ν) and average flame temperature (T_{flame}) of the composite sticks were determined from the macroscopic videos. The linear burn rate was calculated by dividing the length of the sample (3 cm) by the burning time observed with the macroscopic video. Steady burning was achieved quickly, nominally with <1 mm of sample being consumed before reaching steady state. The heat flux calculations

consider densities (ρ), burn rates (ν), and flame temperatures (heat flux $\sim \rho \times \nu \times T$)²⁷ and are normalized assuming that they have the same specific heat capacity of different samples (eqs S1–S3 and Tables S8–S10). The details of how we obtained the temperature by color pyrometry can be found in our previous studies.^{55,56} Briefly, three channel intensity (red, green, and blue) ratios extracted from a color camera are processed using a house-built MATLAB routine and demosaiced for the camera's Bayer filter using standard MATLAB algorithms. The system was calibrated with a blackbody source (Mikron, Oriel), and the corresponding flame temperature maps were output and reported. The temperature uncertainty is estimated to be ~200–300 K.

3. RESULTS AND DISCUSSION

3.1. Embedding Carbon Fibers into a High Loading Al/CuO Nanothermite. Carbon fibers with a diameter of ~7 μm and a maximum length of ~3 mm (SEM images and brief physical properties are found in Figure S1 and Table S1, respectively) were embedded into high loading (~90 wt %) Al/CuO nanothermite-printed sticks through a direct writing technique. The detailed ink formulations are summarized in Tables S2 and S6.

As shown in Figure 2a, the carbon fibers are randomly dispersed in the ink and extruded through a blunt stainless-steel needle with an inner diameter of ~1.2 mm (16 gauge). As illustrated in Figure 2b, since the carbon fibers are longer than the inner diameter of the needle (>1.2 mm), they are aligned when passing through the needle during the printing process (Figure 2b).^{45–48,51} The morphology of the Al/CuO prints with embedded carbon fibers are depicted in an illustration, and an optical microscopy image is shown in Figure 2c. A cross-sectional SEM image (Figure 2d) shows that the carbon fibers are generally embedded parallel to the direction of writing. More evidence of the predominantly parallel alignment

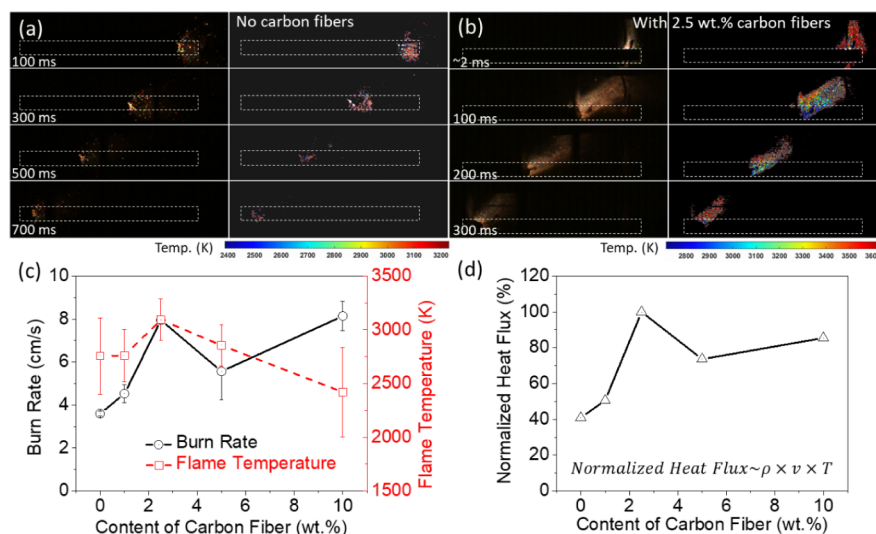


Figure 3. Macroscopic imaging snapshots of Al/CuO (Al/CuO is ~ 82 – 90 wt %, varying with different carbon fibers; details are given in Table S1) composites without (a) and with 2.5 wt % (b) aligned carbon fibers. Summary of the burn rates and mean flame temperatures (c). The normalized heat flux (d) of Al/CuO composite prints with different contents of carbon fibers (details are found in Table S9). The equivalence ratio of Al/CuO in this figure is 0.8. **Note:** The marked squares are where the Al/CuO-printed sticks were located.

of the carbon fibers in the Al/CuO composites is revealed when the printed sticks are viewed from different angles in the SEM (Figure 2e–g).

The composites sticks were also printed with different contents of carbon fibers. Their respective SEM images are shown in Figure S2. The measured and theoretical densities/porosities of the Al/CuO composite sticks with different carbon fibers contents are summarized in Table S3.

3.2. Macroscopic Imaging: Enhanced Propagation of Al/CuO Composites with Carbon Fibers. Al/CuO composites with varied carbon fiber content (0, 1, 2.5, 5, and 10 wt %) were printed (cut into 3 cm long sticks, with a height of ~ 1 mm and a width of ~ 2 mm) and investigated by measuring propagation rates and flame temperatures in an inert atmosphere (1 atm argon). As shown in Figure 1, the macroscopic propagation events were recorded by a high-speed color camera with light exposure settings optimized to obtain the most color information while avoiding overexposure. Figure 3a,b shows the typical time-resolved snapshots, from which we could obtain the flame propagation rates. The flame temperature of the combustion events was measured using three-color pyrometry,^{55,56} and the corresponding temperature maps are shown in Figure 3a,b. From these images, one can see an ~ 350 K variation in the flame temperature for materials with different amounts of carbon fiber addition. However, the change is relatively minor considering the errors in the measurement.

The propagation rates (average burn rate ν = total stick length/total burn time) and the average flame temperatures (T = an average of all active points in a whole burning event) of the Al/CuO composites with different amounts of carbon fibers are summarized and shown in Figure 3c. With an increase in carbon fiber content from 0 to 2.5 wt %, the burn rate rapidly increases from ~ 3.5 to ~ 8 cm/s and fluctuates from ~ 6 to 8 cm/s when the carbon fiber content is ≥ 5 wt % (typical macroscopic videos are summarized in Video S1). This result supports the hypothesis of an increase in the burn rate with the carbon fiber addition. With an increase in the carbon fiber content, flame temperatures peak at ~ 2.5 wt % and

decrease gradually from ~ 3100 to ~ 2400 K with an increase in the carbon fiber content. Combined with measured densities (ρ , Table S3) of the prints, we can estimate a normalized heat flux ($\sim \rho \times \nu \times T$, detailed in the Supporting Information) and summarize the results in Figure 3d, which shows that ~ 2.5 wt % carbon fiber addition enhances the heat flux of the Al/CuO composites by $\sim 250\%$. Although the snapshots in Figure 3a,b indicates that the flames are larger in the composites without carbon fiber additives, the apparent change in heat release suggests that there may be other interactions or modes of heat transfer on smaller length scales, which are difficult to resolve with the macroscopic imaging apparatus (~ 70 $\mu\text{m}/\text{pixel}$).

3.3. Microscopic Imaging: Enhanced Heat Feedback and Heat Transfer with Carbon Fibers. To probe reaction dynamics at the flame front, a high-resolution microscopic imaging system (~ 1.7 $\mu\text{m}/\text{pixel}$) coupled with pyrometry software was employed to closely observe the reaction in a small area of ~ 1 mm^2 . As seen in Figure 4a, the reference Al/CuO composites without any carbon fiber addition show growing agglomerations on the burning surface that is up to

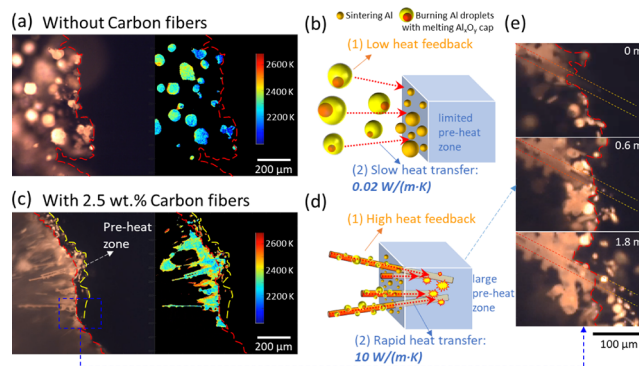


Figure 4. Microscopic imaging of Al/CuO composite prints without (a) and with 2.5 wt % (c) carbon fibers. The corresponding cartoons (b,d) illustrate heat feedback to the preheat zone. The heated carbon fibers are seen to be inducing the new ignition sites in the preheat zone (e). The propagation is from left to right.

~100 μm . As shown in Figure 4a,b, since most of the hot agglomerations fly away from the burning surface, the heat feedback from these particles to the unreacted material will be relatively low and slow in comparison to those particles that are in physical contact and within the local proximity with the reacting surface. By contrast, the embedded carbon fibers (2.5 wt %, Figure 4c) appear to “catch” particles that were being ejected. With the hot particles being closer to and in physical contact with the reacting surface, it is reasonable to expect that the heat feedback increases in those cases with carbon fibers.

A long-existing challenge in Al-based energetics, especially in aluminized solid propellants, is the exhaust Al_xO_y plume that plays a significant role in combustion performance, causing two-phase losses that reduce the specific impulse.^{57–59} It is well documented that Al nanoparticles start to sinter (agglomerate) when the temperature is near its melting point (933 K).^{42,57–60} Further studies focusing on aluminum-integrated propellant grains have observed aluminum/alumina agglomerates growing (coalescing) into micro-sized spheres on the burning surface.^{42,57–60} Al droplet vaporization (Al boiling point: ~2743 K) induces the droplets ($\text{Al}/\text{Al}_x\text{O}_y$ droplets with Al_xO_y smoke) to detach from the burning surface.^{42,58} The enhanced heat feedback from the inclusion of carbon fibers (Figure 3c) allows the temperature along the reaction front (red dash lines) to reach as high as ~2400–2600 K, ~400 K higher as compared to the reference case (Figure 3a). If the temperature of the reaction front is high enough (Figure 3c,d, >2400 K), the small droplets leave the surface without further coalescing into the droplets as large as the reference case; this is a phenomenon observed in our previous study.⁴² From these results, one could conjecture that these embedded carbon fibers might help to reduce the two-phase losses of the aluminized propellants.

In principle, the addition of carbon fibers might also affect the heat transfer in the composites.^{61–63} The thermal conductivity of carbon fiber can vary widely from ~10 to ~1000 $\text{W}\cdot\text{m}^{-1}\cdot\text{K}^{-1}$, while the value of carbon fibers used in this study is estimated to be ~10–20 $\text{W}\cdot\text{m}^{-1}\cdot\text{K}^{-1}$.^{62,63} A ~2.5 wt % addition of the carbon fibers, however, should not appreciably increase the calculated overall thermal conductivity/diffusivity, until a fiber conductivity of at least ~250 $\text{W}\cdot\text{m}^{-1}\cdot\text{K}^{-1}$ (~aluminum's thermal conductivity), as shown in Figure S3 and Table S4. Although the addition of carbon fibers might not increase the overall thermal conductivity of the composites, conductive heat transfer from hot burned/burning particles to the unburnt materials via these fibers might be quite efficient, especially in the case where the carbon fibers themselves create a connective network (Figure 4d).⁴⁷ However, while the average conductivity might not be substantially impacted (because of its small mass fraction in the composite), the fact remains that the fibers have a much higher thermal conductivity (>10 $\text{W}\cdot\text{m}^{-1}\cdot\text{K}^{-1}$) than the polymer matrix (~0.2 $\text{W}\cdot\text{m}^{-1}\cdot\text{K}^{-1}$) and the surrounding gas (~0.02 $\text{W}\cdot\text{m}^{-1}\cdot\text{K}^{-1}$),^{50,61–64} which provides 10 \times higher overall thermal conductivity (see detailed calculations in Figure S4 and Table S5) through the gas/carbon fiber combination route (0.17 $\text{W}\cdot\text{m}^{-1}\cdot\text{K}^{-1}$, Table S5), compared to those via just gas heat transfer (0.017 $\text{W}\cdot\text{m}^{-1}\cdot\text{K}^{-1}$, Table S5). It is also reasonable to expect that the fibers provide a local path for hot spots perhaps penetrating deep into the preheat zone of the composite. Indeed, observations in Figure 3e show bright spots residing well before the flame front (~50 to 100 μm , a zone between red and yellow dash lines in Figure 3c)

suggestive of earlier ignition points, not observed without fibers. At this point, the evidence is not sufficiently clear to state categorically that this is in fact occurring, but it does warrant further investigation.

To assess whether any unintentional changes were made to the chemistry with the addition of carbon fibers, TG/DSC tests were conducted on the Al/CuO composite sticks with and without carbon fibers in argon at a heating rate of 10 $^\circ\text{C}/\text{min}$ to 1000 $^\circ\text{C}$ (Figure S5). We observed no signatures that would indicate that any additional chemistry was taking place upon fiber addition. In addition, postcombustion analysis of the residue characterized by SEM shows that carbon fibers remain intact after combustion with no evidence of size/shape changes (Figure S5).

3.4. Effects of Equivalence Ratio and Carbon Fiber Addition on Propagation. Al/CuO composites of varied equivalence ratios ($7 \geq \Phi \geq 0.8$, formulations in Table S6) with and without carbon fibers (~2.5 wt %) were investigated using the macroscopic and microscopic imaging systems. Cross-sectional SEM images, measured densities, and porosities are shown in Figure S6 and Tables S7 and S8, respectively. The obtained burn rates, flame temperatures, and normalized heat flux are summarized in Figures 5 and S7 (numbers are

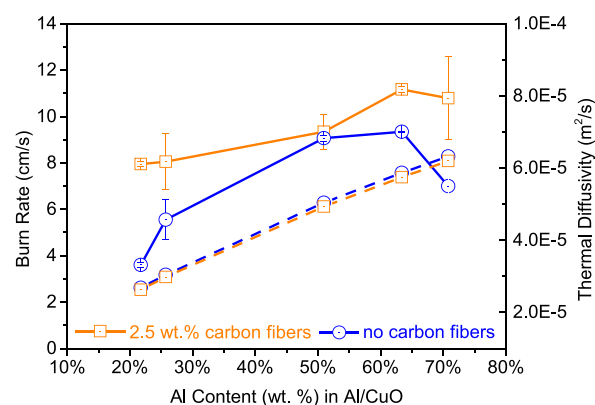


Figure 5. Burn rates (solid lines) and calculated thermal diffusivities (dash lines, calculation details are found in the Supporting Information, and the calculation principle is found in ref 65 of Al/CuO (90 wt %) composite sticks with various equivalence ratios with and without carbon fibers (2.5 wt %).

summarized in Tables S10 and S11). Figure 5 shows that adding fibers increases burn rates in all cases, despite the lower Al/CuO nanothermite loadings (~88 vs ~90 wt %, Table S6).

As we know, thermites generally have higher reactivity when they are mildly fuel rich, which is believed to be due to the enhanced heat transfer from increased concentration of higher thermal conductive Al.⁴⁵ Figure 5 shows that this trend holds for both the neat and the fiber-embedded composites. So while the addition of fibers does not appear to impact the overall thermal conductivity, the burn rates of Al/CuO composites with carbon fibers are all higher than their counterparts regardless of the different equivalence ratios, thus confirming the enhancement of carbon fibers on the propagation of nanothermites by holding reactive particles closer to the unburned surface and providing local, highly conductive pathways.

4. CONCLUSIONS

In this work, carbon fibers were embedded into ~90 wt % loading Al/CuO nanothermite sticks that were fabricated via extrusion direct writing. With only ~2.5 wt % carbon fiber addition, the burn rate and heat flux of the sticks were more than doubled. In situ observation on microscopic combustion finds that carbon fibers effectively trap hot agglomerates, which could contribute to enhance heat feedback to the unreacted material. Composite sticks with and without carbon fibers at different equivalence ratios were also investigated, and the results also confirm the enhancement of the carbon fibers on the combustion performance. This study may provide a new means to enhance the propagation and reduce the two-phase flow loss of 3D-printed composite energetics.

■ ASSOCIATED CONTENT

SI Supporting Information

The Supporting Information is available free of charge at <https://pubs.acs.org/doi/10.1021/acsami.1c02911>.

High-speed macroscopic and microscopic imaging videos of Al/CuO composite sticks with different contents of carbon fibers (Videos S1 and S2) (MP4)-(MP4)

SEM images with different views of carbon fibers and printed Al/CuO sticks with different mass loadings of carbon fibers; cross-sectional SEM images of Al/CuO sticks with various equivalence ratios with and without carbon fibers; TG/DSC results of composites sticks with different mass loadings of carbon fibers; detailed formulations and physical properties include density and porosities of carbon fibers and printed sticks; summary of burn rates, flame temperatures, and heat flux of printed sticks; detailed calculation process for heat flux and thermal diffusivities (PDF)

■ AUTHOR INFORMATION

Corresponding Author

Michael R. Zachariah – Department of Chemical and Environmental Engineering, The University of California Riverside, Riverside, California 92521, United States; orcid.org/0000-0002-4115-3324; Email: mrz@enr.ucr.edu

Authors

Haiyang Wang – Department of Chemical and Environmental Engineering, The University of California Riverside, Riverside, California 92521, United States; orcid.org/0000-0001-5200-3965

Dylan J. Kline – Department of Chemical and Environmental Engineering, The University of California Riverside, Riverside, California 92521, United States; Department of Chemical and Biomolecular Engineering, University of Maryland, College Park, Maryland 20742, United States

Miles C. Rehwoldt – Department of Chemical and Environmental Engineering, The University of California Riverside, Riverside, California 92521, United States; Department of Chemical and Biomolecular Engineering, University of Maryland, College Park, Maryland 20742, United States

Complete contact information is available at: <https://pubs.acs.org/doi/10.1021/acsami.1c02911>

Author Contributions

M.R.Z. initiated and supervised the research. H.W. prepared the samples and carried out the characterization, combustion measurements, and analysis. D.J.K. developed the temperature measurement code. M.C.R. helped with the thermal calculations. H.W. prepared the manuscript, and all the authors made comments on the manuscript. All authors have given approval to the final version of the manuscript.

Notes

The authors declare no competing financial interest.

■ ACKNOWLEDGMENTS

We gratefully acknowledge support from AFOSR. We also thank the CFAMM at the University of California, Riverside, for their microscopy support.

■ REFERENCES

- (1) Wang, Q.; Feng, X.; Wang, S.; Song, N.; Chen, Y.; Tong, W.; Han, Y.; Yang, L.; Wang, B. Metal-Organic Framework Templated Synthesis of Copper Azide as the Primary Explosive with Low Electrostatic Sensitivity and Excellent Initiation Ability. *Adv. Mater.* **2016**, *28*, 5837–5843.
- (2) Agrawal, J. P. Recent Trends in High-Energy Materials. *Prog. Energy Combust. Sci.* **1998**, *24*, 1–30.
- (3) Sikder, A. K.; Sikder, N. A. Review of Advanced High Performance, Insensitive and Thermally Stable Energetic Materials Emerging for Military and Space Applications. *J. Hazard. Mater.* **2004**, *112*, 1–15.
- (4) Ma, X.; Li, Y.; Hussain, I.; Shen, R.; Yang, G.; Zhang, K. Core-Shell Structured Nanoenergetic Materials: Preparation and Fundamental Properties. *Adv. Mater.* **2020**, *32*, No. 2001291.
- (5) Dubrovin, A. S.; Slepova, L. V.; Kuznetsov, V. L. Effect of Density on the Combustion of Aluminothermic Compositions. *Combust., Explos. Shock Waves* **1970**, *6*, 60–67.
- (6) Pantoya, M. L.; Levitas, V. I.; Granier, J. J.; Henderson, J. B. Effect of Bulk Density on Reaction Propagation in Nanothermites and Micron Thermites. *J. Propul. Power* **2009**, *25*, 465–470.
- (7) Ahn, J. Y.; Kim, J. H.; Kim, J. M.; Lee, D. W.; Park, J. K.; Lee, D.; Kim, S. H. Combustion Characteristics of High-Energy Al/CuO Composite Powders: The Role of Oxidizer Structure and Pellet Density. *Powder Technol.* **2013**, *241*, 67–73.
- (8) Wainwright, E. R.; Weihs, T. P. Microstructure and Ignition Mechanisms of Reactive Aluminum–Zirconium Ball Milled Composite Metal Powders as a Function of Particle Size. *J. Mater. Sci.* **2020**, *55*, 14243–14263.
- (9) Sundaram, D.; Yang, V.; Yetter, R. A. Metal-based Nanoenergetic Materials: Synthesis, Properties, and Applications. *Prog. Energy Combust. Sci.* **2017**, *61*, 293–365.
- (10) Mursalat, M.; Hastings, D. L.; Schoenitz, M.; Dreizin, E. L. Microspheres with Diverse Material Compositions can be Prepared by Mechanical Milling. *Adv. Eng. Mater.* **2020**, *22*, No. 1901204.
- (11) Wang, C.; Xu, J.; Dai, J.; Wang, Y.; Shen, Y.; Zhang, Z.; Shen, R.; Ye, Y. Probing the Reaction Mechanism of Al/CuO Nanocomposites Doped with Ammonium Perchlorate. *Nanotechnology* **2020**, *31*, No. 255401.
- (12) He, W.; Lyu, J.; Tang, D.; He, G.; Liu, P.; Yan, Q. Control the Combustion Behavior of Solid Propellants by Using Core-Shell Al-Based Composites. *Combust. Flame* **2020**, *221*, 441–452.
- (13) Calais, T.; Bancaud, A.; Esteve, A.; Rossi, C. Correlation between DNA Self-Assembly Kinetics, Microstructure, and Thermal Properties of Tunable Highly Energetic Al–CuO Nanocomposites for Microprotechnic Applications. *ACS Appl. Nano Mater.* **2018**, *9*, 4716–4725.
- (14) Thiruvengadathan, R.; Bezmelnitsyn, A.; Apperson, S.; Staley, C.; Redner, P.; Balas, W.; Nicolich, S.; Kapoor, D.; Gangopadhyay, K.; Gangopadhyay, S. Combustion characteristics of novel hybrid nanoenergetic formulations. *Combust. Flame* **2011**, *158*, 964–978.

- (15) Comet, M.; Martin, C.; Klamünzer, M.; Schnell, F.; Spitzer, D. Energetic nanocomposites for detonation initiation in high explosives without primary explosives. *Appl. Phys. Lett.* **2015**, *107*, No. 243108.
- (16) Comet, M.; Martin, C.; Schnell, F.; Spitzer, D. Nanothermites: A short review. Factsheet for experimenters, present and future challenges. *Propellants, Explos., Pyrotech.* **2019**, *44*, 18–36.
- (17) Keerthi, V.; Nie, H.; Pisharath, S.; Hng, H. H. Combustion Characteristics of Fluoropolymer Coated Boron Powders. *Combust. Sci. Technol.* **2020**, 1–6.
- (18) Valluri, S. K.; Schoenitz, M.; Dreizin, E. Bismuth Fluoride-Coated Boron Powders as Enhanced Fuels. *Combust. Flame* **2020**, *221*, 1–10.
- (19) Ao, W.; Fan, Z.; Liu, L.; An, Y.; Ren, J.; Zhao, M.; Liu, P.; Li, L. K. B. Agglomeration and Combustion Characteristics of Solid Composite Propellants Containing Aluminum-Based Alloys. *Combust. Flame* **2020**, *220*, 288–297.
- (20) Dennis, C.; Bojko, B. On the Combustion of Heterogeneous AP/HTPB Composite Propellants: A Review. *Fuel* **2019**, *254*, No. 115646.
- (21) McClain, M. S.; Afriat, A.; Rhoads, J. F.; Gunduz, I. E.; Son, S. F. Development and Characterization of a Photopolymeric Binder for Additively Manufactured Composite Solid Propellant Using Vibration Assisted Printing. *Propellants, Explos., Pyrotech.* **2020**, *45*, 853–863.
- (22) Wang, H.; Rehwoldt, M.; Kline, D. J.; Wu, T.; Wang, P.; Zachariah, M. R. Comparison Study of the Ignition and Combustion Characteristics of Directly-Written Al/PVDF, Al/Viton and Al/THV Composites. *Combust. Flame* **2019**, *201*, 181–186.
- (23) Comet, M.; Martin, C.; Schnell, F.; Spitzer, D. Nanothermite foams: From nanopowder to object. *Chem. Eng. J.* **2017**, *15*, 807–812.
- (24) Nagendra, K.; Vijay, C.; Ramakrishna, P. A. Binder Melt: Quantification Using SEM/EDS and its Effects on Composite Solid Propellant Combustion. *Proc. Combust. Inst.* **2019**, *37*, 3151–3158.
- (25) Chatragadda, K.; Vargeese, A. A. Synergistically Catalysed Pyrolysis of Hydroxyl Terminated Polybutadiene Binder in Composite Propellants and Burn Rate Enhancement by Free-Standing CuO Nanoparticles. *Combust. Flame* **2017**, *182*, 28–35.
- (26) Huang, S.; Hong, S.; Su, Y.; Jiang, Y.; Fukushima, S.; Gill, T. M.; Yilmaz, N. E. D.; Tiwari, S.; Nomura, K.; Kalia, R. K.; Nakano, A.; Shimojo, F.; Vashishta, P.; Chen, M.; Zheng, X. Enhancing Combustion Performance of Nano-Al/PVDF Composites with β -PVDF. *Combust. Flame* **2020**, *219*, 467–477.
- (27) Wang, H.; Kline, D. J.; Rehwoldt, M.; Wu, T.; Zhao, W.; Wang, X.; Zachariah, M. R. Architecture Can Significantly Alter the Energy Release Rate from Nanocomposite Energetics. *ACS Appl. Polym. Mater.* **2019**, *1*, 982–989.
- (28) Rehwoldt, M. C.; Wang, H.; Kline, D. J.; Wu, T.; Eckman, N.; Wang, P.; Agrawal, N. R.; Zachariah, M. R. Ignition and Combustion Analysis of Direct Write Fabricated Aluminum/Metal Oxide/PVDF Films. *Combust. Flame* **2020**, *211*, 260–269.
- (29) McClain, M. S.; Gunduz, I. E.; Son, S. F. Additive Manufacturing of Ammonium Perchlorate Composite Propellant with High Solids Loadings. *Proc. Combust. Inst.* **2019**, *37*, 3135–3142.
- (30) He, Z.; Xia, Z.; Hu, J.; Ma, L.; Li, Y. Effects of Aluminum and Temperature on the Tensile Mechanical Properties of Lithium-Perchlorate/Polyvinyl Alcohol-Based Electrically Controlled Solid Propellants. *Propellants, Explos., Pyrotech.* **2020**, *3*, 493–502.
- (31) Wainwright, E. R.; Dean, S. W.; Lakshman, S. V.; Weihs, T. P.; Gottfried, J. L. Evaluating Compositional Effects on the Laser-Induced Combustion and Shock Velocities of Al/Zr-Based Composite Fuels. *Combust. Flame* **2020**, *213*, 357–368.
- (32) Mez, A. G.; Eri Ken, C.; Yilmazer, L.; Pekel, F.; Zkar, S. Mechanical and Burning Properties of Highly Loaded Composite Propellants. *J. Appl. Polym. Sci.* **1998**, *67*, 1457–1464.
- (33) Huang, C.; Jian, G.; DeLisio, J. B.; Wang, H.; Zachariah, M. R. Electrospray Deposition of Energetic Polymer Nanocomposites with High Mass Particle Loadings: A Prelude to 3D Printing of Rocket Motors. *Adv. Eng. Mater.* **2015**, *17*, 95–101.
- (34) Shen, J.; Wang, H.; Kline, D. J.; Yang, Y.; Wang, X.; Rehwoldt, M.; Wu, T.; Holdren, S.; Zachariah, M. R. Combustion of 3D Printed 90 wt% Loading Reinforced Nanothermite. *Combust. Flame* **2020**, *215*, 86–92.
- (35) Wang, Y.; Luo, T.; Song, X.; Li, F. Electrospinning Preparation of NC/GAP/Submicron-HNS Energetic Composite Fiber and its Properties. *ACS Omega* **2019**, *4*, 14261–14271.
- (36) Cheng, L.; Yang, H.; Yang, Y.; Li, Y.; Meng, Y.; Li, Y.; Song, D.; Chen, H.; Artiaga, R. Preparation of B/Nitrocellulose/Fe Particles and Their Effect on The Performance of an Ammonium Perchlorate Propellant. *Combust. Flame* **2020**, *211*, 456–464.
- (37) Ruz-Nuglo, F. D.; Groven, L. J. 3-D Printing and Development of Fluoropolymer Based Reactive Inks. *Adv. Eng. Mater.* **2018**, *20*, No. 1700390.
- (38) Fehlberg, S.; Örneke, M.; Manship, T. D.; Son, S. F. Decomposition of Ammonium-Perchlorate-Encapsulated Nanoscale and Micron-Scale Catalyst Particles. *J. Propul. Power* **2020**, *36*, 862–868.
- (39) Pang, W.; DeLuca, L. T.; Fan, X.; Glotov, O. G.; Wang, K.; Qin, Z.; Zhao, F. Combustion Behavior of AP/HTPB/Al Composite Propellant Containing Hydroborate Iron Compound. *Combust. Flame* **2020**, *220*, 157–167.
- (40) Kubota, N.; Ichida, M.; Fujisawa, T. Combustion Processes of Propellants with Embedded Metal Wires. *AIAA J.* **1982**, *20*, 116–121.
- (41) Isert, S.; Lane, C. D.; Gunduz, I. E.; Son, S. F. Tailoring Burning Rates Using Reactive Wires in Composite Solid Rocket Propellants. *Proc. Combust. Inst.* **2017**, *2*, 2283–2290.
- (42) Wang, H.; Kline, D. J.; Biswas, P.; Zachariah, M. R. Connecting Agglomeration and Burn Rate in a Thermite Reaction: Role of Oxidizer Morphology. *Combust. Flame* **2021**, *231*, No. 111492.
- (43) Golobic, A. M.; Durban, M. D.; Fisher, S. E.; Grapes, M. D.; Ortega, J. M.; Spadaccini, C. M.; Duoss, E. B.; Gash, A. E.; Sullivan, K. T. Active Mixing of Reactive Materials for 3D Printing. *Adv. Eng. Mater.* **2019**, *21*, No. 1900147.
- (44) Westphal, E. R.; Murray, A. K.; McConnell, M. P.; Fleck, T. J.; Chiu, G. T. C.; Rhoads, J. F.; Gunduz, I. E.; Son, S. F. The Effects of Confinement on the Fracturing Performance of Printed Nanothermites. *Propellants, Explos., Pyrotech.* **2019**, *1*, 47–54.
- (45) Wang, H.; Shen, J.; Kline, D. J.; Eckman, N.; Agrawal, N. R.; Wu, T.; Wang, P.; Zachariah, M. R. Direct Writing of a 90 Wt% Particle Loading Nanothermite. *Adv. Mater.* **2019**, *31*, No. 1806575.
- (46) Wang, H.; Biswas, P.; Kline, D. J.; Zachariah, M. R. (2021) Flame Stand-off Effects on Propagation of 3D Printed 94 wt.% Nanosized Pyrolants Loading Composites. *Environmental and Chemical Engineering*, University of California Riverside, manuscript submitted for publication.
- (47) Rehwoldt, M. C.; Kline, D. J.; Zachariah, M. R. Numerically Evaluating Energetic Composite Flame Propagation with Thermally Conductive, High Aspect Ratio Fillers. *Chem. Eng. Sci.* **2020**, *229*, No. 116087.
- (48) Lewicki, J. P.; Rodriguez, J. N.; Zhu, C.; Worsley, M. A.; Wu, A. S.; Kanarska, Y.; Horn, J. D.; Duoss, E. B.; Ortega, J. M.; Elmer, W.; Hensleigh, R. 3D-printing of Meso-structurally Ordered Carbon Fiber/Polymer Composites with Unprecedented Orthotropic Physical Properties. *Sci. Rep.* **2017**, *7*, No. 43401.
- (49) Li, N.; Li, Y.; Liu, S. Rapid Prototyping of Continuous Carbon Fiber Reinforced Poly(lactic Acid) Composites by 3D Printing. *J. Mater. Process. Technol.* **2016**, *238*, 218–225.
- (50) Love, L. J.; Kunc, V.; Rios, O.; Duty, C. E.; Elliott, A. M.; Post, B. K.; Smith, R. J.; Blue, C. A. The Importance of Carbon Fiber to Polymer Additive Manufacturing. *J. Mater. Res.* **2014**, *29*, 1893–1898.
- (51) Tekinalp, H. L.; Kunc, V.; Velez-Garcia, G. M.; Duty, C. E.; Love, L. J.; Naskar, A. K.; Blue, C. A.; Ozcan, S. Highly Oriented Carbon Fiber–Polymer Composites via Additive Manufacturing. *Compos. Sci. Technol.* **2014**, *105*, 144–150.
- (52) Yi, Z.; Cao, Y.; Yuan, J.; Mary, C.; Wan, Z.; Li, Y.; Zhu, C.; Zhang, L.; Zhu, S. Functionalized Carbon Fibers Assembly With Al/Bi₂O₃: A New Strategy For High-Reliability Ignition. *Chem. Eng. J.* **2020**, *389*, No. 124254.

(53) Siegert, B.; Comet, M.; Muller, O.; Pourroy, G.; Spitzer, D. Reduced-sensitivity nanothermites containing manganese oxide filled carbon nanofibers. *J. Phys. Chem. C* **2010**, *114*, 19562–19568.

(54) Elder, B.; Neupane, R.; Tokita, E.; Ghosh, U.; Hales, S.; Kong, Y. L. Nanomaterial Patterning in 3D Printing. *Adv. Mater.* **2020**, *32*, No. 1907142.

(55) Jacob, R. J.; Kline, D. J.; Zachariah, M. R. High Speed 2-Dimensional Temperature Measurements of Nanothermite Composites: Probing Thermal vs. Gas Generation Effects. *J. Appl. Phys.* **2018**, *123*, No. 115902.

(56) Kline, D. J.; Alibay, Z.; Rehwoldt, M. C.; Idrogo-Lam, A.; Hamilton, S. G.; Biswas, P.; Xu, F.; Zachariah, M. R. Experimental Observation of the Heat Transfer Mechanisms that Drive Propagation in Additively Manufactured Energetic Materials. *Combust. Flame* **2020**, *215*, 417–424.

(57) Chakraborty, P.; Zachariah, M. R. Do Nanoenergetic Particles Remain Nano-Sized during Combustion? *Combust. Flame* **2014**, *161*, 1408–1416.

(58) Chen, Y.; Guildenbecher, D. R.; Hoffmeister, K. N.; Cooper, M. A.; Stauffacher, H. L.; Oliver, M. S.; Washburn, E. B. Study of Aluminum Particle Combustion in Solid Propellant Plumes Using Digital In-Line Holography and Imaging Pyrometry. *Combust. Flame* **2017**, *182*, 225–237.

(59) Karasev, V. V.; Onischuk, A. A.; Glotov, O. G.; Baklanov, A. M.; Maryasov, A. G.; Zarko, V. E.; Panfilov, V. N.; Levykin, A. I.; Sabelfeld, K. K. Formation of Charged Aggregates of Al₂O₃ Nanoparticles by Combustion of Aluminum Droplets in Air. *Combust. Flame* **2004**, *138*, 40–54.

(60) Lengellé, G.; Duterque, J.; Trubert, J. F. Combustion of Solid Propellants. In *RTO/VKI Special Course on Internal Aerodynamics in Solid Rocket Propulsion*, Rhode-Saint-Genèse, Belgium, May 27–31, 2002; RTO-EN-023-4, 2002; pp 1–62.

(61) Shen, J.; Liu, Z.; Xu, B.; Liang, H.; Zhu, Y.; Liao, X.; Wang, Z. Influence of Carbon Nanofibers on Thermal and Mechanical Properties of NC-TEGDN-RDX Triple-Base Gun Propellants. *Propellants, Explos., Pyrotech.* **2019**, *44*, 355–361.

(62) Pradere, C.; Batsale, J. C.; Goyhèneche, J. M.; Pailler, R.; Dilhaire, S. Thermal Properties of Carbon Fibers at Very High Temperature. *Carbon* **2009**, *3*, 737–743.

(63) Wang, M.; Kang, Q.; Pan, N. Thermal Conductivity Enhancement of Carbon Fiber Composites. *Appl. Therm. Eng.* **2009**, *2-3*, 418–421.

(64) Zhou, W.; Zuo, J.; Ren, W. Thermal Conductivity and Dielectric Properties of Al/PVDF Composites. *Composites, Part A* **2012**, *4*, 658–664.

(65) Progelhof, R. C.; Throne, J. L.; Ruetsch, R. R. Methods for predicting the thermal conductivity of composite systems: A review. *Polym. Eng. Sci.* **1976**, *16*, 615–625.